Cerebral Cortex April 2007;17:803-815
doi:10.1093/cercor/bhk033
Advance Access publication May 12, 2006

Timing of Muscle Activation in a Hand Movement Sequence

Mary D. Klein Breteler[1,2], Katarzyna J. Simura[1] and Martha Flanders[1]

[1]Department of Neuroscience, University of Minnesota, Minneapolis, MN 55455, USA and [2]Department of Cognitive Psychology, Nijmegen Institute for Cognition and Information, Radboud University, Nijmegen, The Netherlands

Recent studies have described muscle synergies as overlapping, multimuscle groups defined by synchronous covariation in activation intensity. A different approach regards a synergy as a fixed temporal sequence of bursts of activity across groups of motoneurons. To pursue this latter definition, the present study used a principal component (PC) analysis tailored to reveal the across-muscle temporal synergies of human hand movement. Electromyographic (EMG) activity was recorded as subjects used a manual alphabet to spell a list of words. The analysis was applied to the EMG waveforms from 27 letter-to-letter transitions of equal duration. The first PC (of 27) represented the main temporal synergy; after practice, it began to account for more of the EMG variance (up to 40%). This main synergy began with a burst in the 4-finger extensor and a silent period in the flexors. There were then progressively later and shorter bursts in the thumb abductor, thumb flexor, little finger abductor, and finally the finger flexors. The results suggest that hand movements may be generated by activity waves unfolding in time. Because finger muscles are under relatively direct cortical control, this suggests a specific form of cortical pattern generation.

Keywords: electromyography, fingerspelling, individuation, muscle synergy, temporal synergy

Introduction

Recent research has reopened the issue of muscle synergies. In the 1980s, the main question was the extent to which activation combinations were flexible or fixed (Nashner 1977; Buchanan and others 1986; Soechting and Lacquaniti 1989; Macpherson 1991). More recently, the goal has been to determine the extent to which each muscle participates in each synergy and to quantify the number of synergies needed to account for a particular motor pattern. For example, it has been determined that about 6 muscle synergies can almost fully account for the electromyographic (EMG) activity of about 12 frog leg muscles during various behaviors (Tresch and others 1999; Saltiel and others 2001; Hart and Giszter 2004). Somewhat akin to the traditional concept of central pattern generators for mammalian gait, scratching, etc., these frog muscle synergies are thought to represent the output of distinct, modular, premotor drives in the spinal cord (Bizzi and others 1995, 2000).

The distinction between "synchronous synergies" and "time-varying synergies" for the control of frog leg movements had been introduced by d'Avella and Bizzi (2005). A synchronous synergy is a vector of weighting coefficients that specify the relative involvement (strength of membership) of each muscle in the group. In contrast, a time-varying synergy is a collection of EMG bursts in various muscles. The bursts may be of different intensity and duration for the different muscles, but the muscle membership and temporal pattern are fixed for each synergy (see also d'Avella and others 2003). d'Avella and Bizzi (2005) explained that several synchronous synergies may be scaled by a different amount at each point in time and then summed together to fit the EMG data for a particular movement. However, unless all muscles in a given synergy normally burst in synchrony, a different analytical approach is needed to identify the invariant temporal patterning of EMG bursts in a data set. In the present study, we used such an approach to identify the across-muscle temporal muscle synergies for human hand movements.

Although finger movements may be fundamentally different from locomotor activity (being under more direct cortical control), synergy analysis is a useful approach. Hand movements have been characterized in terms of synchronous muscle synergies (Holdefer and Miller 2002; Brochier and others 2004; Weiss and Flanders 2004), but the temporal muscle synergies remain to be identified. Santello and others (2002) applied a temporal synergy analysis to the sequence of joint rotations involved in reaching to grasp 20 different objects. These investigators found that the temporal pattern was well characterized as the weighted sum of 2 orthogonal components: 1) an extension/abduction and then flexion/adduction of all joints in unison and 2) a monotonic progression from the current to the final joint angles, serving to precisely shape the hand to the specific object in the second half of the reach. The present study used a similar temporal synergy analysis on the EMG data from a hand movement sequence, that of American Sign Language (ASL) fingerspelling.

Fingerspelling is a well-specified task that features a rich variety of postural transitions. Our group has proposed that the study of fingerspelling movements, coupled with studies of reaching to grasp various objects and keyboard positioning movements, represents a comprehensive set of tasks in which humans skillfully make individuated finger movements without having significant force interactions with external objects. As partially mentioned above, we have previously characterized the patterns of joint rotations for all these tasks (Santello and others 1989, 2002; Soechting and Flanders 1997; Jerde and others 2003a, 2003b) as well as the synchronous muscle synergies for static grasping and fingerspelling hand shapes (Weiss and Flanders 2004). For our initial study of temporal muscle synergies, we chose to focus on dynamic fingerspelling movements, a task that is both rhythmic and complex. We reasoned that the rhythmicity would allow us to align and scale our EMG data into discrete segments (for averaging and analysis), and the complexity would insure that we would observe a realistic

amount of individuation in the finger movements. We recorded EMG as nonfluent human subjects practiced using the ASL manual alphabet to spell a list of words. We sought to quantitatively describe the EMG temporal patterns in terms of coactivation and reciprocal activation of pairs of muscles (relative amplitude fluctuations), as well as the relative onset times and burst durations. Thus, we sought to reveal the invariant across-muscle temporal synergies.

Materials and Methods

Subjects

Nine human subjects (6 males and 3 females, mean age 29) participated in our experiment after giving informed consent. To determine the extent of hand dominance, each was asked to fill out the Edinburgh Handedness Inventory (Oldfield 1971). Six subjects were right handed (mean score +78), and 3 were left handed (mean score −72). None of the subjects were fluent signers. However, they were given ample opportunity to become familiar with the hand shapes that represent the 26 letters of the ASL manual alphabet.

Task and Procedure

The subjects were comfortably seated with the elbow of the dominant arm on an armrest. Each was asked to finger spell words that were presented on a computer screen. An entire set of hand shapes was presented graphically, with the printed letters underneath, as in the top row of Figure 1. These words were chosen to contain a wide range of hand shape transitions. The spelling of each word started and ended with a neutral, relaxed hand shape. Each block of trials consisted of spelling each of the 6 words listed in Figure 1 seven times in a row, with a pause in between the words/trials, that is, WHITE 7 times, followed by TIE 7 times, etc. Thus, each block contained 42 trials.

There were 7 blocks of dynamic spelling trials, which were used to examine changes in the EMG patterns across skill acquisition. These 7 blocks were alternated with 8 groups of static trials (starting and ending with a group of static trials). In the static trials, all letters (n = 14) occurring in the 6 words were presented one at a time in random order and the shape was held for 2 s. These trials were intended to help the subjects learn (by providing rest and reinforcement), and the EMG data were used to control for recording stability (as explained below). Subjects were allowed as much rest as they wanted in between blocks or words to prevent fatigue. We stressed to subjects that during spelling, they were not allowed to produce force with their fingers against other fingers, for example, they were told not to squeeze when making a fist. Ideally, all force produced by the hand muscles was supposed to go into moving the fingers or holding the hand in a specific shape.

Data Acquisition

Hand Shape

Subjects wore either a left-handed or a right-handed version of an instrumented glove (Cyberglove, Virtual Technologies, Palo Alto, CA), depending on hand dominance. The glove was individually calibrated for each subject using a standard set of postures. We recorded from 17 sensors with an angular resolution of <0.5° and a temporal resolution of 12 ms. The measured angles were the metacarpal phalangeal and proximal interphalangeal (PIP) joint angles for the thumb and the 4 fingers; abduction of the thumb, middle, ring, and little fingers; thumb rotation; and wrist pitch and yaw.

Muscle Activity

Small bipolar Ag/AgCl electrodes were attached to cleaned and abraded skin. The conductive surfaces were 2 mm in diameter, and the disk centers were positioned 10 mm apart. (Permanent electrodes similar to our discontinued SensorMedics set are currently available from Discount Disposables, St. Albans, VT.) The electrodes were custom soldered to shielded cable and led to customized A-M Systems EMG amplifiers. The ground was connected to the contralateral wrist. Muscle activity was amplified and band-pass filtered (60–500 Hz). EMG signals from 8 channels were digitized at 1000 samples per second.

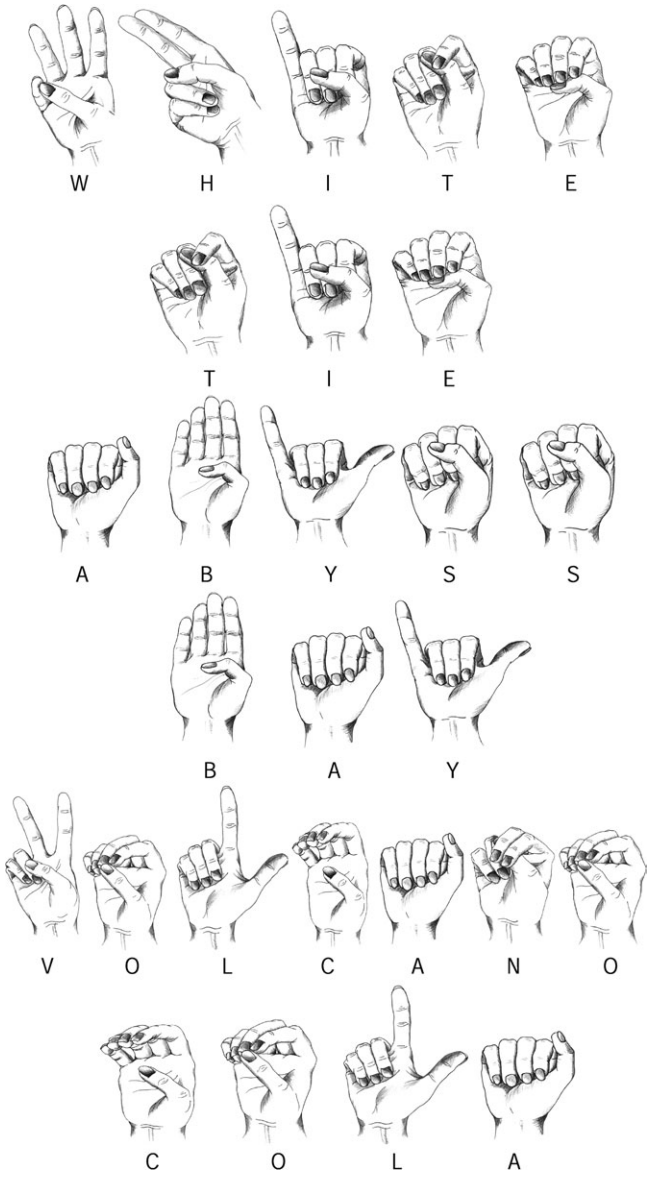

Figure 1. The ASL hand shapes of the words spelled in each of the 7 blocks of trials. During the experiment, a picture of the letters and hand shapes of the current word to be spelled (e.g., one row of this figure) was presented to the subject on the computer screen. In each block of trials, the subjects spelled WHITE 7 times and then TIE 7 times, followed by 7 trials each with the words ABYSS, BAY, VOLCANO, and COLA.

We recorded surface EMG from the same sites as illustrated in our previous study of static hand shapes (Fig. 1 of Weiss and Flanders 2004). We recorded from 2 parts of the first dorsal interosseus: the part near the thumb (DIT) and the part closer to the metacarpal of the index finger (DIF). On the palmar side of the thumb, we recorded from abductor pollicis brevis (APB) and flexor pollicis brevis (FPB). The other intrinsic muscle was the abductor digiti minimi (ADM), a muscle that is well isolated from other muscles and moves only the little finger.

We also recorded from some of the extrinsic muscles that act upon all 4 fingers. The flexor digitorum superficialis (FDS), a forearm muscle that flexes all fingers, is a difficult muscle for recordings with surface electrodes because it is partly hidden underneath other muscles and tendons. The recording locations for this muscle were consistent with our previous publication (Weiss and Flanders 2004) but different from those suggested in older literature. After conducting a cadaver study and a preliminary recording study with numerous electrode placements, we decided to place one set of electrodes (FD) 25% of the distance from the

wrist crease to the elbow crease between the tendons of palmaris longus and flexor carpi radialis (Fig. 2, recording location a). We placed a second set (FD2) about 33% of the distance from the wrist crease to the elbow crease on the ulnar side of the palmaris longus tendon (Fig. 2, recording location b). This positioned the electrodes directly over FDS but did not allow for separate recordings from digit-specific FDS compartments. In test maneuvers involving rhythmical, voluntary flexion–extension of individual PIP joints, our FD electrode recorded mostly from the middle finger portion of FDS (Fig. 2, top row), whereas the FD2 electrode picked up more activity during movements of the other 3 fingers (Fig. 2, second row). Figure 2 also shows test recordings from locations recommended for fine-wire (index finger FDS) electrodes (location c, Burgar and others 1997) and for surface (4-finger flexor) electrodes (location d, Basmajian and Blumenstein 1989). The present study did not use these locations due to the relatively large amount of EMG recorded during wrist flexion (middle right panel of Fig. 2), presumably due to the close proximity of flexor carpi radialis and the other wrist flexors (lower left panel of Fig. 2).

Using the eighth EMG channel, we recorded from the 4-finger extensor, extensor digitorum (ED). For simplicity, the 4 EMG channels devoted to DIT, DIF, FD, and FD2 will be referred to as representing 4 different "muscles" even though they really represent different parts of 2 muscles. For the remaining 4 muscles, we placed a single bipolar electrode pair over the middle portion of the muscle.

Compared with most conventional EMG systems, our bipolar surface electrodes were very small and closely spaced. We assume that they recorded from the motor units directly under the electrode with the largest amplitudes and from more distant motor units with peak amplitudes that decayed exponentially with distance (Basmajian and De Luca 1985). In our previous study with the same surface electrodes (Weiss and Flanders 2004), we showed that the same unit could be identified on the DIT and DIF electrodes (possibly due to overlapping

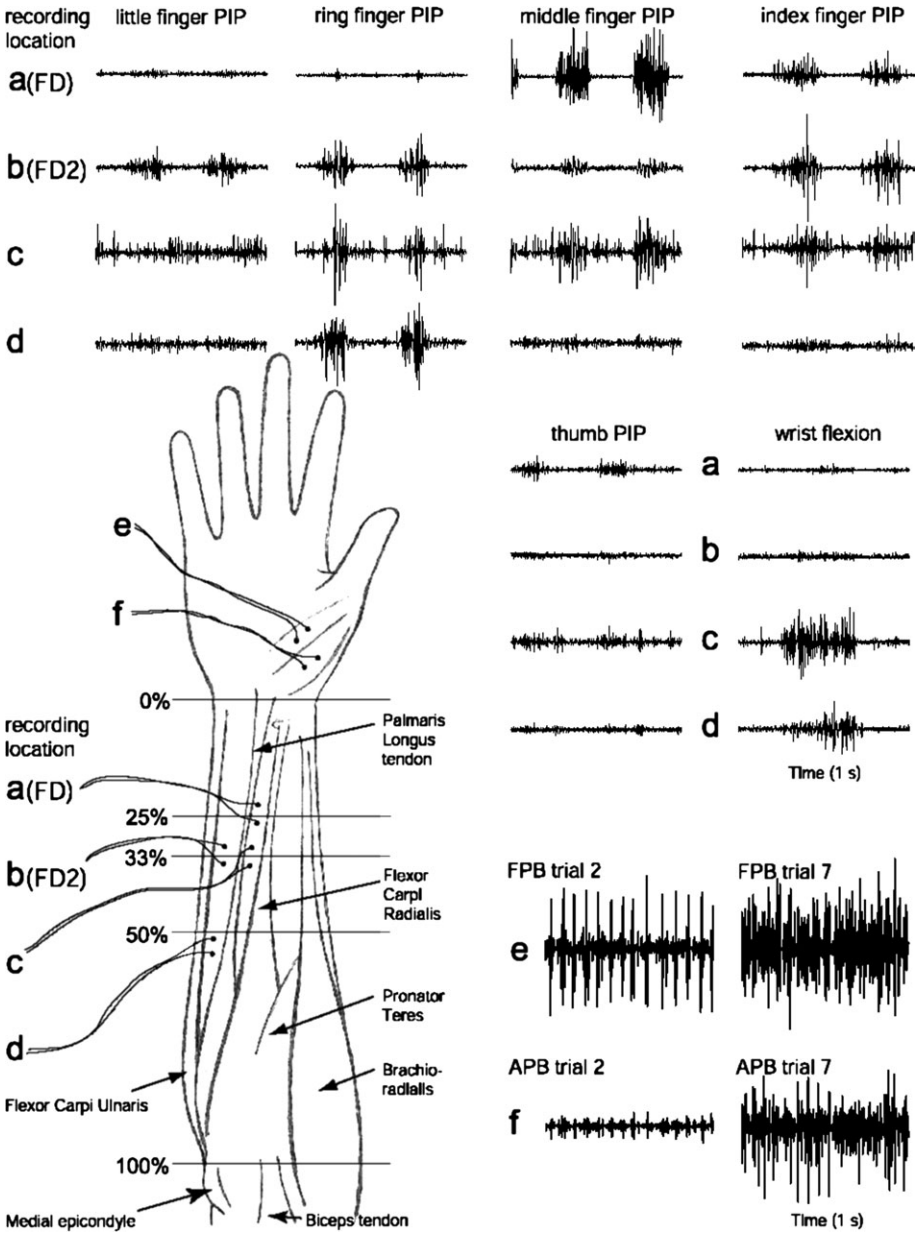

Figure 2. A demonstration of our choice of FDS (FD and FD2) recording locations (rows a, b, c, and d), and an evaluation of the degree of cross talk recorded from APB electrodes during the firing of an FPB motor unit (rows e and f, left panels, trial 2 of Weiss and Flanders 2004). During a trial involving a different static hand shape, these 2 thumb EMG channels showed similar overall amplitudes (rows e and f, right panels, trial 7 of Weiss and Flanders 2004). On the anatomical illustration (lower left panel), the bipolar electrode spacing (1 cm) is drawn to scale. Thus, the APB and FPB recording locations were separated by 2 cm.

fiber fields as well as the close distance). However, the other channels appeared to be well separated. For the present study, to quantify the extent to which our APB electrode recorded FPB units (and vice versa), we reanalyzed data from 7 units previously isolated from the surface EMG with a template-matching algorithm (listed in Table 3 of Weiss and Flanders 2004). In 4 of the 7 cases, the identified unit could not be seen in the (less than 2 cm distant) EMG recording from the adjacent muscle. In the other 3 cases, the amplitude decrement was on average 84% (±8% standard deviation). A representative example of this level of cross talk is shown in the lower right panel of Figure 2.

We defer further comments on EMG technical considerations to the Discussion, but note here that the number of independent EMG channels (8, 7, or 6) had no bearing on the main results of this analysis. This is because the temporal synergy analysis combined data from each EMG channel separately across the 27 movements (instead of combining data across the 8 EMG channels).

Data Analysis

Processing Cyberglove Data

The Cyberglove data were used in 2 ways. First, we checked that the words were spelled correctly, that is, that the right sequence of hand shapes was produced. For viewing images of the recorded hand shapes, we rendered the Cyberglove data using Persistence of Vision Ray Tracer (copyrighted freeware). Second, because subjects paused for each letter, we segmented the signals into letter transitions using the minima of the summed, rectified joint angular velocity traces (see Jerde and others 2003b). This is illustrated in the upper part of Figure 3. After recording the actual transition times, each letter transition was time normalized to 100 samples. The time-normalized velocity traces of the 7 consecutive trials of the same word were then correlated with one another, and the best 5 trials (i.e., the ones having the highest mean correlation to the other trials) were selected for the subsequent EMG analysis. This allowed us to remove the occasional error trials while maintaining the same number of trials in each EMG average.

Processing EMG Signals

For the dynamic spelling trials, the EMG signals were rectified and then the sample frequency was reduced by taking the average values of each 5 consecutive data points (i.e., each 5 ms). Next, the signal was digitally smoothed using a 2-sided exponential filter with a time constant of 5 ms.

For each static (control) trial, the average rectified EMG amplitude was calculated. As in our previous study (Weiss and Flanders 2004), the average values of the static trials were used to insure that there were no sudden changes in the amplitude of the EMG signal across the 1- to 2-h-long experimental session. Unfortunately, this did happen in 5 of the 72 cases (8 EMGs × 9 subjects) and was usually a single event (probably triggered by sweating in the glove, followed by a movement that broke the closest seal of the adhesive around the gel-covered 2-mm conductive surface). Four of the 5 cases were thumb muscles (APB or FPB). The change in static EMG levels before and after the dynamic block was then used to correct the amplitude gain of the EMG from the dynamic trials (average scale factor = 7.0 ± 4.7).

The dynamic EMG signals from each letter transition were time normalized (by resampling to 100 data points) between each of the transition points measured from the Cyberglove data. (We also used a fixed time shift of 36 ms to account for the electromechanical delay.) As shown in Figure 3 and documented previously (Jerde and others 2003b), letter transitions occur at regular intervals. Thus, the time normalization corrected for the small amount of variability across letters (about 20 ms) as well as the variability across repeat trials (about 10 ms after practice).

For each of the 9 subjects, we then averaged the time-normalized EMG signals of the best 5 repeat trials (selected based on the Cyberglove data, as described above), resulting in a single smooth EMG signal for each muscle, for each letter/word, in each block. For each smooth EMG signal (i.e., for each of the 8 channels), the minimum value over the entire experiment was subtracted and the maximum value over the entire experiment was used to normalize the peak. This resulted in signals ranging from 0 to 1 for each muscle.

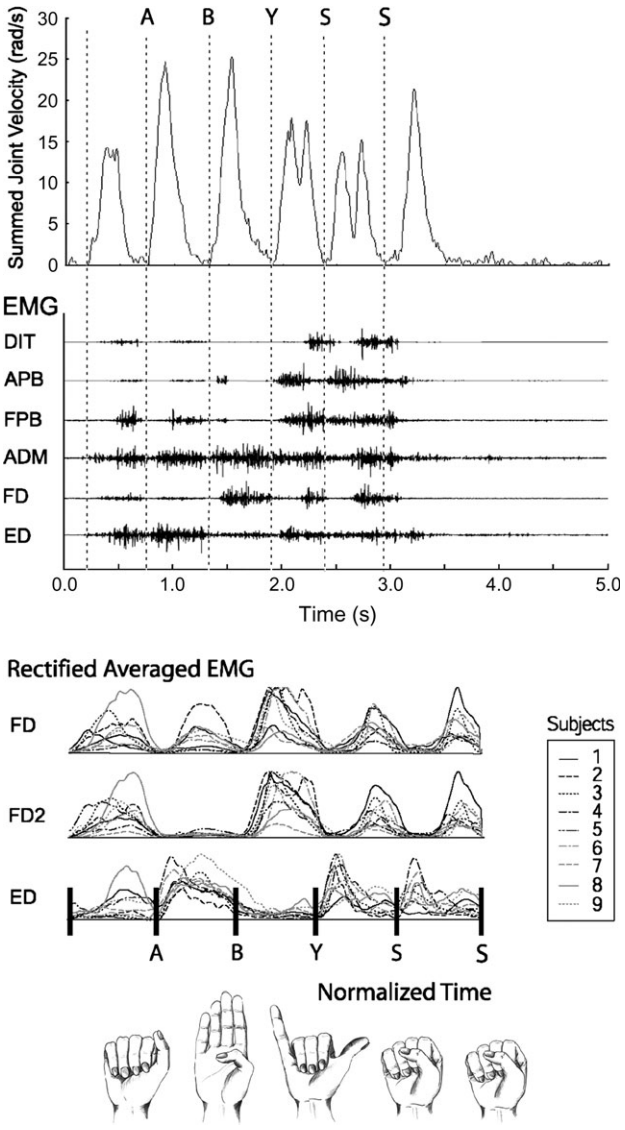

Figure 3. Cyberglove and EMG data from one trial where the subject spelled the word ABYSS. The bottom row shows the target sequence of hand shapes. The top panel shows the rectified joint angular velocity (rad/s), summed over all joints for one trial; subjects typically paused for each letter. Based on the minima of this trace, the trial was segmented (dashed vertical lines) into transitions between letters. The next panel shows the muscle activity recorded from 6 of the 8 EMG channels, for this trial. The muscles were DIT, APB, FPB, ADM, flexor digitorum superficialis (FD), and ED. The lower panel also shows EMG data from a second channel on FDS (FD2) and shows processed EMG data from all 9 subjects, for 3 EMG channels. These EMG data were rectified, smoothed, time normalized based on the velocity segments, and then averaged (across trials and blocks). Notice the difference between FD and FD2 during the A to B transition and the reciprocal relation between FD/FD2 and ED activity.

For the analysis of skill acquisition, we examined the EMG pattern in each of the 7 practice blocks. In all other cases, a grand mean EMG signal was calculated by averaging the last 5 blocks, where a relatively stable EMG pattern was observed. Before analyzing the pattern across muscles, the grand mean for each muscle was normalized to its maximum value (see Figs 3 and 4).

Principal Component Analysis

We used principal component (PC) analysis to find the most common multimuscle burst patterns across the 27 letter transitions (the "temporal synergies"). As mentioned in the Introduction, patterns of covariation across primate hand muscles have previously been found

using a synchronous synergy analysis (Holdefer and Miller 2002; Brochier and others 2004; Weiss and Flanders 2004). Thus, the main goal of the present study was to focus on the temporal aspects of bursting patterns (i.e., the temporal synergies). However, for comparison (in Fig. 10), we also applied a synchronous synergy analysis.

To delineate the temporal synergies, we designed an analytical approach aimed at revealing the main activation waveforms of the 8 muscles, linked by their concurrent presence in the 27 letter transitions. We also tried independent component analysis for comparison (data not shown) but settled on PC analysis without rotation to provide a ranked orthogonal set of components. Our PC approach is similar to that described by Santello and others (2002), except that the previous study used 15 joint angles and 20 movements and the present study used 8 EMGs and 27 movements. We did a separate analysis for each of the 9 subjects. We did a separate analysis for each of the 7 blocks, and then we also did the analysis using the grand mean from the last 5 blocks.

The input to our temporal synergy PC analysis was the averaged smoothed EMG signal for each muscle, for each letter transition. As illustrated in Figure 4*a*, each of the 27 letter-transition vectors was composed of 8 single-letter EMG waveforms. Figure 4*a* shows the first 5 vectors (top) and last 4 vectors (bottom) that formed the columns of a typical input matrix (5-block grand means from one subject). Figure 4*b* shows the EMG waveforms of the first PC, for the data set in Figure 4*a*.

We did a PC waveform analysis of the type described by Glaser and Ruchkin (1976), using the Matlab "princomp" function (see also Flanders 1991; Santello and others 2002). This analysis results in 27 basic PC waveforms, computed from the 27 × 27 covariance matrix of the 27 letter-transition vectors. The covariance calculation removes the mean from each of the 27 columns of the input matrix. Thus, the 800-point EMG waveforms for each letter (EMG_{letter}, Fig. 4*a*) could be perfectly reconstructed as the average EMG level for each letter (mean EMG_{letter}) plus a weighted sum of the 27 PC waveforms (PC1–PC27, see Fig. 4*b*):

$$EMG_{letter} = \text{mean}\,EMG_{letter} + PC1 \times W1_{letter} + \cdots + PC27 \times W27_{letter}, \quad (1)$$

where $W1_{letter}$–$W27_{letter}$ are the weighting coefficients. The PCs are ranked such that PC1 is most important in the reconstruction of the EMG input data (accounting for the largest portion of the variance). Note that mean EMG_{letter} consists of a single value for each letter rather than a time-varying waveform. Due to this separate term for the average EMG level (mean EMG_{letter}), the 27 PCs contain EMG waveforms that go positive (bursts) and negative (silent periods) around zero (see inset in Fig. 4*b*).

A synchronous synergy analysis is configured in a different manner. In the temporal synergy analysis described by equation (1), each EMG input vector contains the waveforms of all 8 muscles for one letter transition (subscript letter). Thus, the PCs also contain waveforms for each of the 8 muscles linked by their common occurrence in multiple letter transitions. In contrast, in a synchronous synergy analysis, each EMG input vector represents one muscle (subscript muscle, see Fig. 10*a*), and the synchronous muscle synergies are described by the 8 weighting coefficients ($W1_{muscle}$–$W8_{muscle}$, see Fig. 10*c*):

$$EMG_{muscle} = \text{mean}\,EMG_{muscle} + PC1 \times W1_{muscle} + \cdots + PC8 \times W8_{muscle}. \quad (2)$$

Although the examination of the 8 weighting coefficient vectors (Fig. 10*c*) reveals coactive and reciprocal synergies (as in Weiss and Flanders 2004), we will show that the examination of the 8 PCs derived in this manner (Fig. 10*b*) does not reveal invariant temporal patterns. Thus, the 2 types of synergy analysis are complementary.

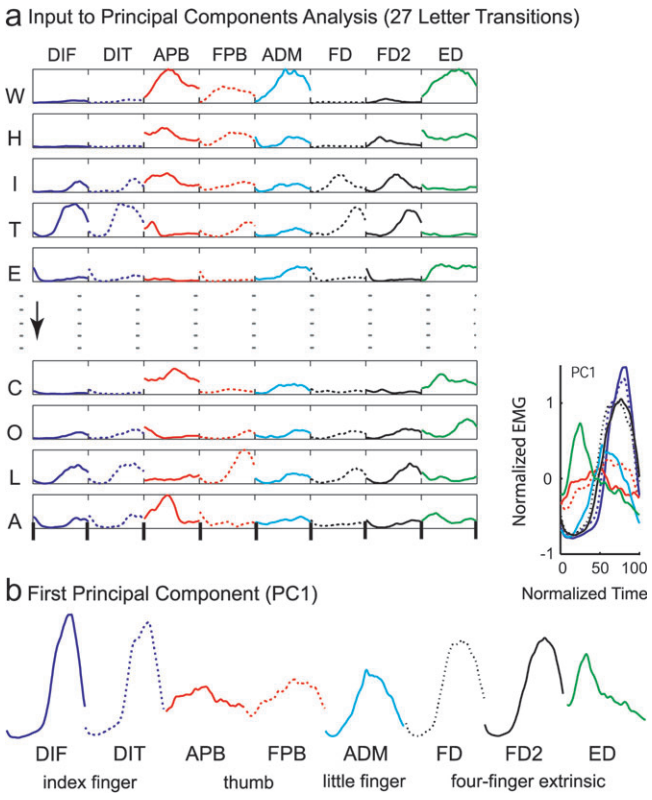

Figure 4. (*a*) An example of the input to the PC analysis used to identify the most common 8-EMG burst combinations (across-muscle temporal synergies). With 27 letter transitions as the input (WHI. . .OLA), the analysis resulted in 27 PCs. PC1 is shown in (*b*), with the color-coded waveforms for the 8 muscles stretched across the panel or (in the inset) overlaid, with 0 representing the average EMG level. The average EMG level plus the weighted combination of the 27 PCs perfectly reconstructed the EMG vector for each letter transition. The analysis was done separately for each subject; these data are from subject 6.

Results

Overview

We used PC analysis to examine the temporal aspects of the EMG pattern. Each of the 27 PCs contained a particular temporal waveform for each muscle (Fig. 4*b*). To compare the burst characteristics across muscles, in most figures we will display the waveforms of the 8 muscles superimposed in the time frame of a single-letter transition (inset to Fig. 4*b*). We will refer to each of the twenty-seven 8-muscle PCs as a temporal synergy, and because they are ranked by percent variance explained, we will focus on the first few temporal synergies. For example, in the first PC (Fig. 4*b*), it is clear that the 4-finger extensor (ED, green line) became active first and the flexors (dark blue and black lines) became active later, with bursts of intermediate timing in the thumb muscles (red lines) and the little finger muscle (turquoise line). This corresponds to the fact that most letter transitions involved opening the hand, rearranging the relative positions of the digits, and closing the hand (see Fig. 1).

Although all 27 PCs are needed to perfectly reconstruct the inputs, the first 4 PCs accounted for almost 80% of the variance, with the first 2 together accounting for about 60% (Table 1). In the sections below, we will demonstrate that PC1 showed a consistent pattern across blocks and that the PC1 and PC2

Table 1
Percent variance explained (mean of 9 subjects ± standard error)

	Block 1	Block 6	Blocks 3–7
PC1	32 ± 9	39 ± 10	37 ± 8
PC2	23 ± 8	21 ± 9	21 ± 7
PC3	12 ± 4	11 ± 2	11 ± 2
PC4	6 ± 1	8 ± 2	8 ± 1
PCs 1–4 combined	73 ± 4	79 ± 1	77 ± 2

waveforms showed similarities across subjects. PC3 and PC4, as well as the higher order components, were much more variable across subjects. Because the main goal of our study was to describe the most consistent features of the temporal patterns in multimuscle burst components, we will focus on the steady-state pattern in the last 5 blocks, for PC1 and PC2. In the final section, for comparison with the temporal synergy analysis, we will subject the EMG data from the last 5 blocks to a synchronous synergy analysis.

Changes in Speed and Percent Variance Explained across Blocks

Several aspects of fingerspelling were relatively stable over the last 5 of the 7 blocks of trials (Fig. 5). In contrast, the speed of the subjects' hand movements improved rapidly across the first 2 blocks. This is quantified in Figure 5*a* (left panel) by showing the grand mean letter-transition times ($n = 9$ subjects) for each block. Transition times were about 850 ms in the first block, and this was significantly different from the times of about 650 ms in blocks 4–7 (analysis of variance [ANOVA] with Scheffé post hoc test, $P < 0.05$).

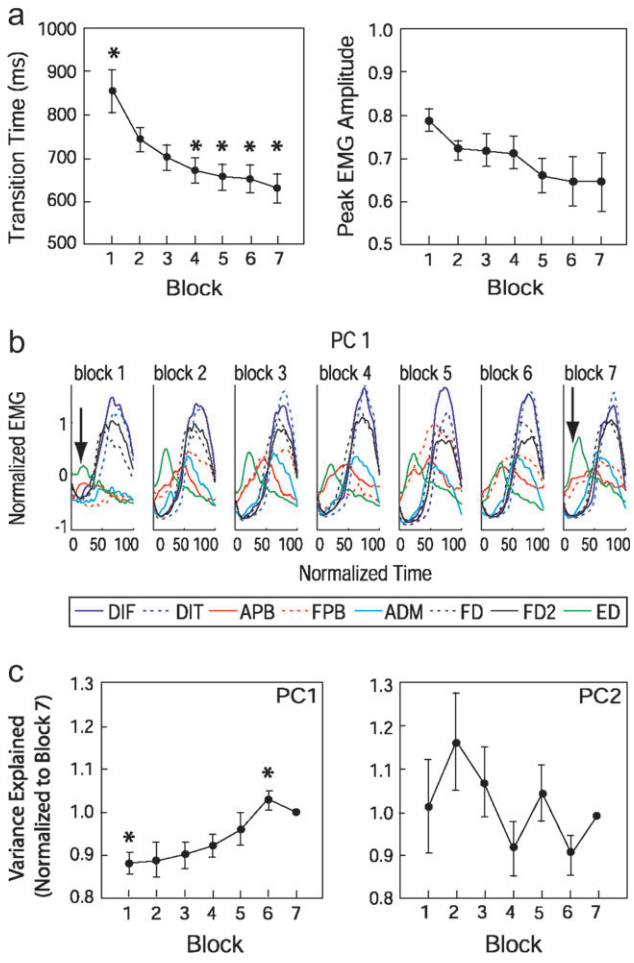

Figure 5. (*a*, left panel) Movement time for the transitions between letters (prior to the time-base normalization). The data were averaged across letters for each subject and then across subject means to produce a grand mean ($n = 9$) and standard error. In the first block, transitions took significantly longer than in the last 4 blocks (*$P < 0.05$). (*a*, right panel). Despite the increase in movement speed with practice, the peak EMG amplitude did not increase. (*b*) The evolution of PC1 over time is shown using data from one subject (subject 6). The arrows indicate that early reciprocal activity (positive early burst of ED, APB, and FPB vs. negative period for all other muscles) became more prominent after the first 2 blocks. (*c*) The variance explained by the first component (left plot) increased over the blocks. The variance explained by PC2 (right plot) was much more variable. These data were combined across subjects ($n = 9$) after being normalized to block 7.

A reduction in transition time, or an increase in speed, would generally be expected to be accompanied by a marked increase in the amplitude of EMG bursts (e.g., Gottlieb and others 1989). However, as subjects began to spell more quickly, the peak EMG amplitudes did not increase. As illustrated in the right panel of Figure 5*a*, grand mean peak EMG amplitudes (averaged across all letters and muscles and then all subjects) did not change significantly. Because technical difficulties tended to produce decreases rather than increases in the EMG gain (see Materials and Methods), as a control, we separately quantified the data from ED, a large forearm muscle with very stable EMG signals. In line with the data from all muscles in Figure 5*a*, ED peak amplitude decreased by 12% from block 1 to block 7; it decreased in 6 subjects and increased in 3 subjects. Thus, it seems reasonable to conclude that peak EMG amplitude generally did not increase with speed.

The fact that subjects began to spell words faster without simply increasing peak EMG activity may suggest a change in the overall EMG pattern. To examine this issue, we computed EMG temporal PCs for each block individually. Figure 5*b* shows, for a representative subject (same subject as in Fig. 4), the progression of PC1 during practice. In blocks 3–7, the early muscle activity clearly represented a reciprocal pattern, where the extensor (ED, green line) contributed a positive burst to the reconstruction of EMG data (activity peaks above the zero mean), whereas the index finger muscle (DIF/DIT, blue lines) and the extrinsic flexors (FD/FD2, black lines) contributed a phasic silent period (activity lows below the zero mean). This early reciprocal activation pattern is indicated by an arrow in the plot for block 7. In contrast, at the very beginning of practice (Fig. 5*b*, block 1), this early reciprocal activity was lacking (arrow).

This tendency for an increase in reciprocal activation was clearly present in the data from at least half of the subjects. However, the exact pattern of waveform changes was quite variable across subjects, and so we did not attempt further quantification. For all subjects, the waveforms that constituted the PC1 pattern appeared to stabilize after the first 2 blocks, and therefore we directed further quantification of the PC1 temporal synergy at the average waveforms across the last 5 blocks.

For PC1, the percent variance explained increased across the learning blocks; on average, the subjects showed a smooth increase in the importance of PC1 across the first 6 blocks (Fig. 5*c*, left plot). The percent variance values (normalized to the last block) for blocks 1 and 6 were significantly different from each other (ANOVA with Scheffé post hoc test, $P < 0.05$). In contrast, for PC2 (Fig. 5*c*, right plot), the change in percent variance explained was much more variable. For PC1–PC4, Table 1 lists the percent variance values for the first block, the sixth block, and the last 5 blocks together. PC1 was the only component that showed a clear change across skill acquisition; changes in PC2–PC4 were more variable.

Temporal Synergies in the Last 5 Blocks

In subsequent sections, we will focus on the 2 main temporal synergies (PC1 and PC2) derived from the grand mean EMG waveforms of the last 5 blocks. However, we will first summarize the contributions of all 27 temporal synergies to the

reconstruction of the EMG waveforms. In Figure 6*a*, we show the results of the temporal PC analysis on the grand mean EMG waveforms from one subject, and in Figure 6*b*, we summarize the percent variance explained for all subjects. In Figure 6*a*, the burst waveforms are scaled according to the range of the weighting coefficients used to reconstruct the EMG data. Thus, PC1 had the largest amplitude, and it is clear that the highest order PCs (e.g., PC27) contributed very little to the reconstruction of the EMG data. PC1 was a pattern where the 4-finger extensor (ED, green line) and the thumb muscles (APB and FPB, red lines) were active early and the other muscles were active later. The higher order components displayed various other temporal patterns, which were variable across subjects. However, it was common for the index finger muscle (DIF/DIT, dark blue lines) and the little finger muscle (ADM, turquoise lines) to show a relatively large amplitude waveform in some of the higher order components (e.g., Fig. 6*a*, PC5 and PC7). Interestingly, in many cases the waveforms of PC1–PC7 resembled sine waves.

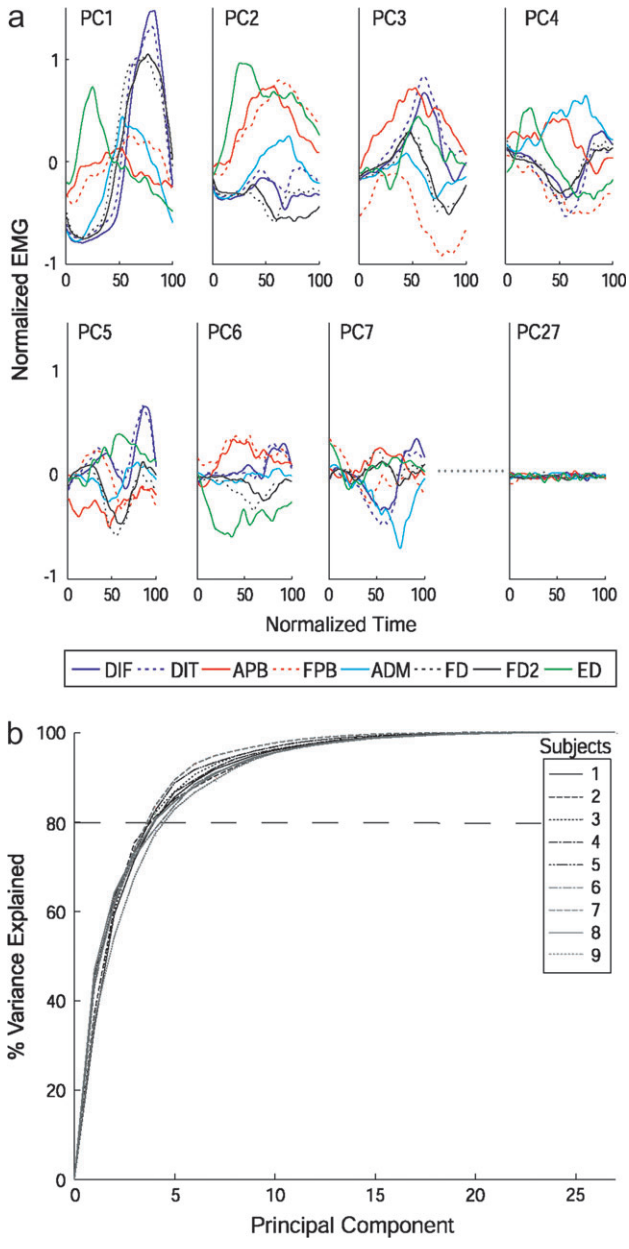

Figure 6. (*a*) Some of the 27 PCs, or across-muscle temporal synergies for subject 6, that formed the output of our synergy analysis. PCs are ranked according to the percent variance explained and are shown scaled by the range of weighting coefficients. Each component consists of 8 EMG waveforms, superimposed to facilitate comparison. (*b*) For each subject (different line styles), about 4 PCs were needed to explain 80% of the variance.

The First 2 Temporal Synergies

In most subjects, PC1 contributed to the reconstruction of most letter transitions with positive weighting coefficients. This is shown for a representative subject in the top panel of Figure 7 (same subject as in Figs 4–6). In contrast, PC2 typically contributed to the reconstruction with either a positive or a negative weighting coefficient, depending on the particular letter transition (Fig. 7, bottom panel). Thus, the EMG pattern for the various letter transitions could be approximated as a sum of PC1 with various positive weights and PC2 with various positive or negative weights.

The subject featured in Figures 4–7 was subject 6. For this subject, the number of positive weighting coefficients (out of 27 possible) was 27 for PC1 and 17 for PC2. As shown in Table 2, for subjects 3–9, PC1 had 23–27 (average = 25) positive weighting coefficients and PC2 had 6–18 (average = 12) positive weighting coefficients. We also noticed common patterns in the sign and value of the weighting coefficients for different letter transitions. For example, for the 4 subjects with 23–25 positive

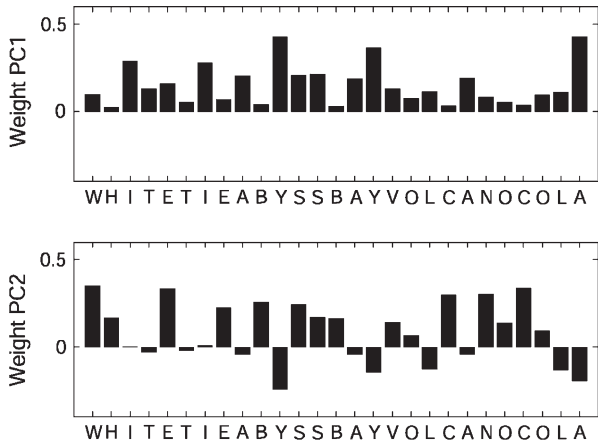

Figure 7. The weighting coefficients for the reconstruction of EMG waveforms for all letter transitions (subject 6). PC1 (top panel) contributed positively to all letter transitions. PC2 (bottom panel) had positive coefficients for some of the letter transitions and negative coefficients for others.

Table 2
Number of positive weighting coefficients (out of 27)

	PC1	PC2
Subject 1	12	27
Subject 2	14	26
Subject 3	27	10
Subject 4	23	18
Subject 5	25	8
Subject 6	27	17
Subject 7	24	6
Subject 8	27	9
Subject 9	25	17

values for PC1, one of the few negative values was always for the I to T transition in WHITE. Unlike most letter transitions, moving from I to T does not involve an initial extension of all fingers (see Fig. 1). Furthermore, for the I to T transition, the PC2 of subjects 3–9 always had a negative weighting coefficient.

Thus, there appeared to be some consistent aspects to the weighting coefficients of the first 2 PCs for subjects 3–9. However, for subjects 1 and 2, the pattern was reversed. In contrast to subjects 3–9 where the average numbers of positive weighting coefficients were 25/12 for PC1/PC2, subjects 1 and 2 had ratios of 12/27 and 14/26, respectively (Table 2). This suggested that the bursting pattern of PC1 in most subjects might be found in PC2 for these subjects (this would simply indicate that the percent variance explained, and thus the ranking, was reversed). We also noticed that PC2 waveforms of subjects 1 and 2 more closely resembled the PC1 waveforms of the other subjects. Therefore, to further examine the characteristics of PC1 and PC2, we reversed the classification of these components for subjects 1 and 2, in order to combine the data across subjects. This created the 2 categories shown in Figure 8, which we will refer to as PCa (Fig. 8, top) and PCb (Fig. 8, bottom).

After this regrouping, for all 9 subjects, the weights of PCa were predominantly positive and the weights of PCb were about equally positive and negative. Furthermore, grouped in this manner, there were similarities across all subjects in the multimuscle bursting patterns. In order to provide a concise description of the PCa and PCb patterns, we quantified these patterns using the analysis presented in Figure 8.

In the top row of Figure 8, we have quantified the PCa pattern for all subjects by correlating the waveform for each muscle with the 2 portions of sine waves that begin and end near zero. To capture both the polarity (positive or negative) and the duration of each EMG burst, we computed its correlation with a full sine wave (i.e., with a period equal to the full transition time = "short" burst) and a half sine wave (i.e., with a half-cycle period equal to the full transition time = "long" burst). These values are plotted on the horizontal and vertical axes, respectively. Each symbol represents one muscle for subject 1 (center panel) and for all subjects combined (right panel). For pairs of muscles, a 180° separation would represent perfectly reciprocal activation and a 0° separation would represent coactivation. The radial distance from the center represents the similarity of each muscle's waveform to the 2 sine waves; if this model fits perfectly, all the data would fall on the perimeter of the unit circle.

The top center plot quantifies the PCa pattern of subject 1 (shown in the top left panel). The APB burst was long in duration (red symbol near the pole representing a long positive burst), and the DIT/DIF bursts were short negative and then short positive (blue symbols at the negative end of the x axis). The EMG waveforms for the other muscles were quantified as being initially negative with intermediate durations (symbols in the upper left quadrant).

A similar PCa pattern can be seen in the combined data from all subjects (top right plot). All EMG waveforms except for one (black symbol near origin) were well correlated with the 2 sine waves, yielding correlation coefficients near +1 or –1. The

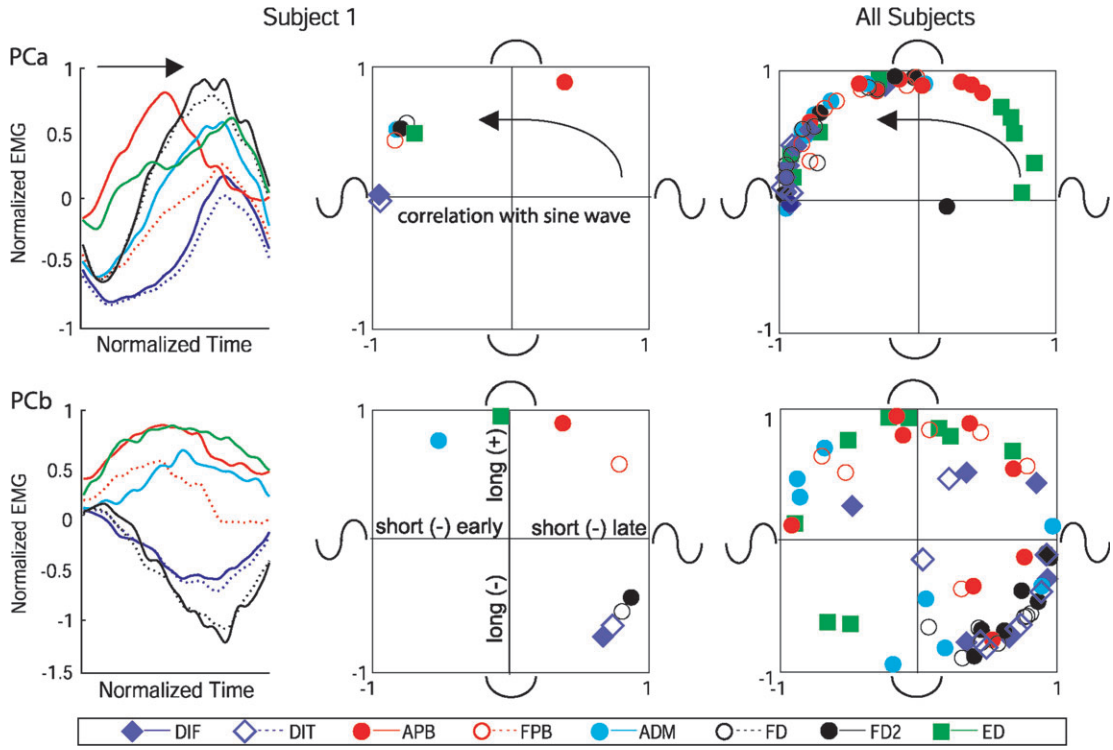

Figure 8. Correlations of the EMG waveforms in PCa and PCb (as shown in the left panels) with sine waves and half sine waves for subject 1 (middle panels) and for all subjects (right panels). The sine wave polarity and duration is indicated at the top, bottom, left, and right of each panel. Each symbol represents the correlation of a single EMG waveform with a sine and a half sine, for example, the turquoise circle in the bottom middle panel shows that the PCb little finger muscle (ADM) of subject 1 had a positive correlation with a half sine and a negative correlation with a full sine wave. Pairs of symbols 180° apart would represent instances of perfectly reciprocal activation. In the upper right panels, the curved arrows represent the progression of burst timing, from a short/early positive burst to a long positive burst to a short/late positive burst.

longest duration burst was positive (i.e., the symbols fell in the upper half of the plot), and both the onset and the duration of the positive burst varied across muscles in a highly consistent manner. For most subjects, as indicated by the curved arrow, the ED burst (green squares) was short and early, followed by a much longer burst in APB (solid red circles), then short bursts in FD/FD2 (black circles), and then DIT/DIF (blue diamonds). The data for the little finger muscle (ADM, turquoise circles) fell in the upper left quadrant, meaning that the waveform began with a short negative period, followed by a positive burst of intermediate duration (as in subject 1, top left panel).

PCb (Fig. 8, bottom row) was quite different from PCa (Fig. 8, top row). Whereas PCa had predominantly positive weighting coefficients (Fig. 7, top) and bursts (Fig. 8, top), PCb had positive and negative weights (Fig. 7, bottom) and bursts (Fig. 8, bottom). Although PCb was less well correlated with sine waves and more variable across subjects (especially for the little finger muscle, ADM, turquoise circles), one feature is particularly noteworthy. As in PCa, data from DIT/DIF (blue diamonds) and FD/FD2 (black circles) were similar to each other. However, in PCb, these data fell in the lower right quadrant, indicating a burst polarity that was usually opposite that of ED (green squares), APB (filled red circles), and FPB (open red circles). This is especially clear in subject 1 (lower left plots in Fig. 7), and it would represent a simple reciprocal pattern, except for the fact that the finger flexor (DIT/DIF, FD/FD2) bursts were generally later and shorter in duration than the thumb muscle and extensor bursts (APB and ED). Thus, in addition to the overriding pattern of reciprocal (extensor–abductor vs. flexor) activation previously noted for muscle synergies in general, our analysis of burst components reveals a continuum of burst onsets and durations.

Averaged PCa Waveforms

For PCa (Fig. 8, top row), our waveform quantification revealed substantial similarity across subjects. The most variable data in the "all subject" plot (right) were those representing ED (green squares), which sometimes fell in the upper right quadrant (indicating a short early burst) and sometimes fell in the upper left quadrant (indicating a short late burst). Qualitative examination of the ED PCa waveforms for all subjects suggested a double-bursting pattern. In most subjects, the first burst was much larger and so the data fell in the upper right quadrant. However, as was the case for subject 1 (Fig. 8, top row), if the second burst was larger, the data fell in the top left quadrant.

Because the PCa waveforms were so similar across subjects, we averaged the data to give a clearer picture of the main temporal synergy. Averaging across subjects is expected to overestimate burst durations but should preserve the relative amplitudes and burst onsets across muscles. In Figure 9, we present this average, plotted in colored lines (as in the previous figures) and also on an intensity plot (middle panel) where blue represents below-average EMG levels, yellow/green represents average levels, and red represents above-average levels. It is apparent that ED (green line and top row) has the longest duration of positive activity and evidence for early and late bursts. APB becomes active next, followed by FPB. The flexors have shorter and later periods of positive activity. Note also that ADM and DIF/DIT have relatively low levels of activity in PCa. This implies that a relatively large positive contribution from the higher order PCs was needed to reconstruct the EMG data from these muscles.

The averaged PCA waveforms for each muscle were fit with sine waves (bottom right panel of Fig. 9). This allowed us to quantify the phase (the temporal location of the symbols at the zero crossings), the frequency or period (half-wave durations shown below the plot), as well as the amplitude and offset (vertical lines).

There are 2 notable instances where the sine waves did not provide good fits. First, in the case of ED (green lines), the double-bursting pattern was poorly fit by a single sine wave. Closer examination of APB and FPB (red lines) suggests the possibility of small secondary bursts in these muscles as well. Second, the initial negative bursts in the data waveforms were not as deep as predicted by the sine wave fits (especially in DIF/DIT, blue lines). This may be related to the inherent limitation of using pauses in positive EMG activity to monitor inhibitory phases in the central pattern (essentially producing a "floor effect" in the data).

Comparison with a Synchronous Synergy Analysis

In the sections above, we used a temporal synergy analysis to reveal the EMG waveforms that are linked by their invariant occurrence together in most letter transitions. Previously, Weiss and Flanders (2004) applied a synchronous synergy analysis to the 26 static hand shapes of the ASL manual alphabet. The results of this analysis were vectors containing the 8 weighting coefficients that signified the contribution of each of the 8 muscles (or EMG channels) to each static (synchronous) muscle synergy. In Figure 10, we present the results of a similar analysis applied not only to the quasistatic hand postures at the transition points but also to all points in time during the finger spelling movements.

As illustrated in Figure 10*a* using data from one subject, the input to this analysis was the 8 EMG signals (grand means in the last 5 blocks) stretched across the normalized time points representing the 27 letter transitions. Because there were 8 EMG vectors as inputs (Fig. 10*a*), there were 8 PCs; the first 3 (PC1, PC2, and PC3) are shown in Figure 10*b*. In each of the 9 subjects, the first 3 PCs together explained more than 80% of the variance in the EMG data.

In Figure 10*c*, we show the extent to which each hand muscle participated in each of the first 3 PCs. For example, for subject 7 (lower right plot), PC1 (solid line) represented coactivation: each of the 8 muscles had positive weighting coefficients. In contrast, PC2 (dashed line) represented a reciprocal pattern, where the sign of the weighting coefficients for the index finger muscle (DIT/DIF) was opposite the sign of the weighting coefficients for the thumb muscles (APB and FPB). This implies that above-average activation of index finger muscles was coupled with below-average activation of thumb muscles. The 4 subjects shown in Figure 10*c* are representative in that we commonly observed a coactivation synergy (all positive or all negative coefficients) and an index finger/thumb reciprocal activation synergy (coefficients with opposite signs) within the first 3 PCs. The basic composition of these muscle synergies is the same as recently reported for static grasping and ASL hand shapes (Weiss and Flanders 2004).

Figure 10*b* also serves to illustrate that this synchronous synergy analysis failed to reveal the temporal synergies. On the right, we show an enlarged and overlaid view of the waveforms for subject 7's PC1 and PC2, for the word VOLCANO. It is apparent that the PC1 and PC2 synergies were expressed with different time courses for different letter transitions. For example, the

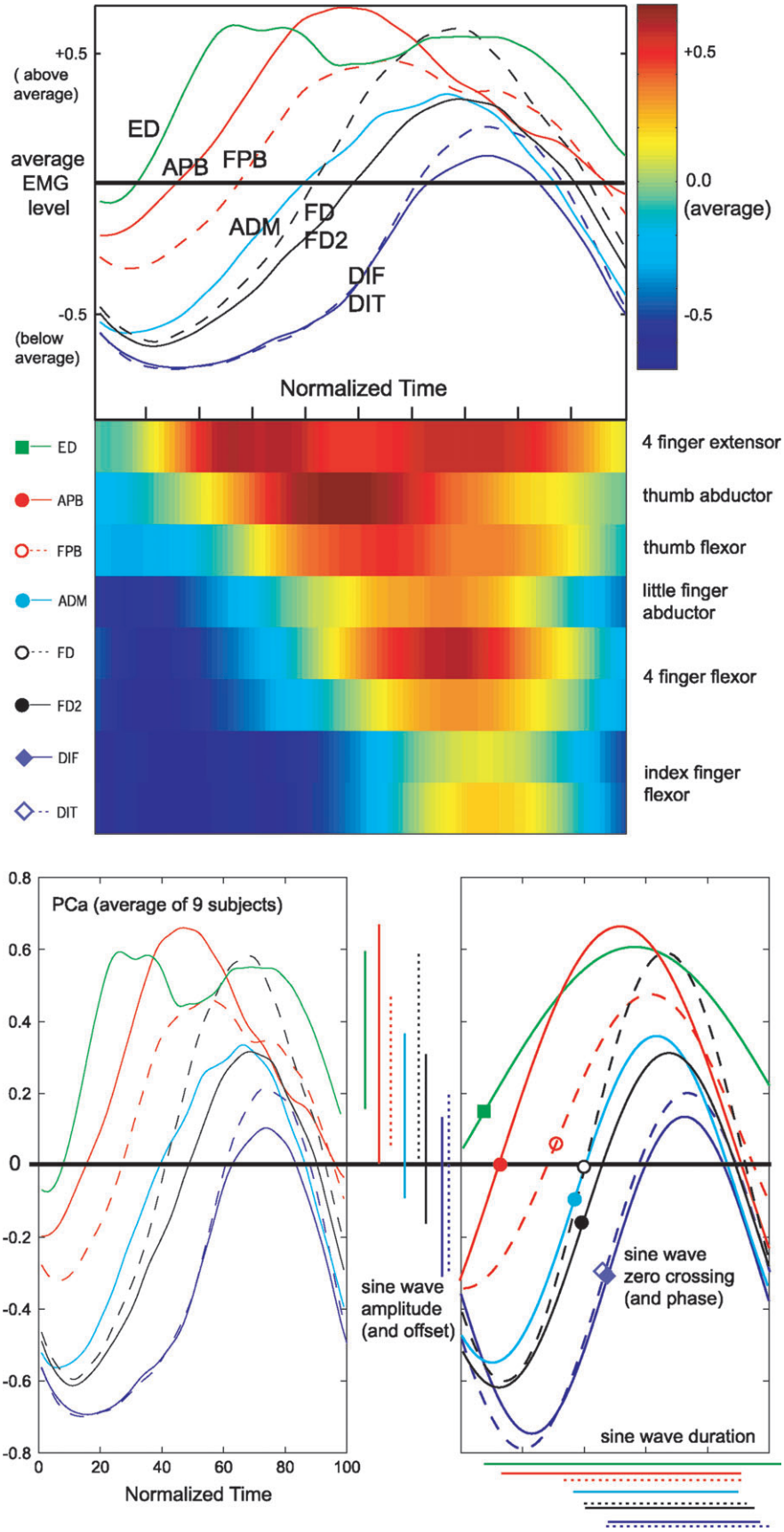

Figure 9. The waveforms representing the main temporal synergy (PCa), averaged across the 9 subjects. In the top panels, the same data are plotted in line and intensity formats. In the bottom panels, these same data are compared with the best-fit sine waves.

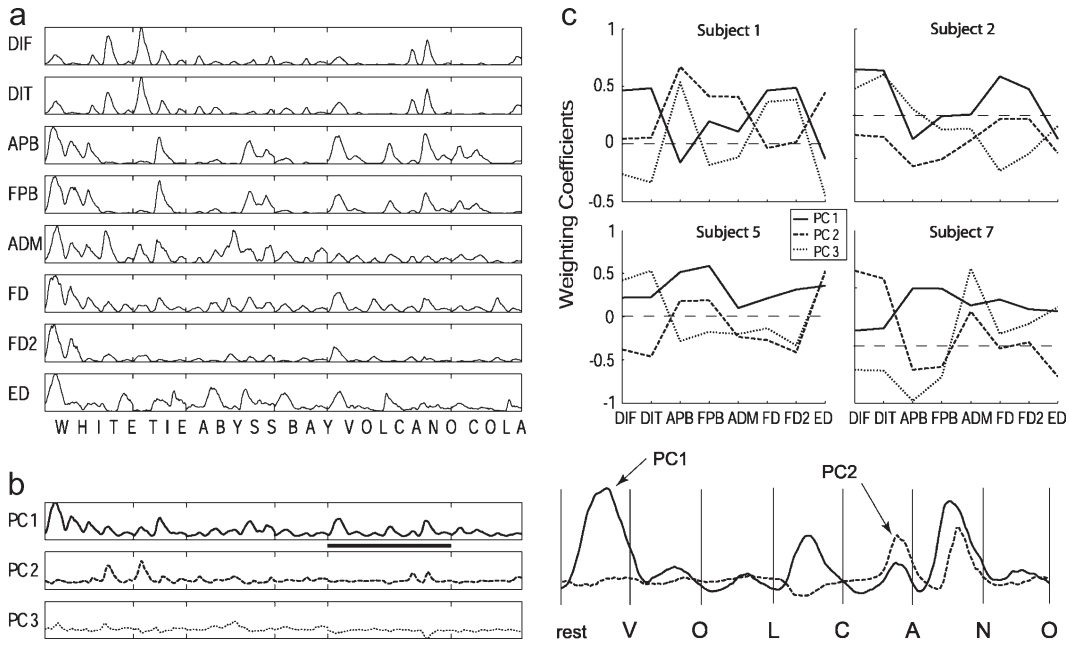

Figure 10. A synchronous synergy analysis was done for comparison. (*a*) The input consisted of the grand mean EMG signals over the last 5 blocks (subject 7). (*b*) The left panel shows the first 3 PCs (PC1, PC2, and PC3); they together explained more than 80% of the variance. The right panel is an enlarged view of a portion of these PC waveforms. (*c*) The synchronous synergies are represented by the weighting coefficients of the 8 muscles (*x* axis) for these first 3 PCs (line styles) for subjects 1, 2, 5, and 7 (in separate panels). In coactive synergies, all muscles were active together (e.g., all positive coefficients for PC1 in subjects 5 and 7, all negative coefficients for PC2 in subject 2). In reciprocal synergies, some muscles had positive coefficients and some had negative coefficients (e.g., PC2 for subjects 5 and 7).

coactive (PC1) synergy peaked near the half way point for rest-V, L-C, and A-N but much later for C-A. The more reciprocal synergy (PC2) showed a late, positive burst for the C-A and A-N transitions but an early inversion for the L-C transition. If this analysis had revealed the same waveforms for each movement (e.g., a half sine wave for PC1 and a full sine wave for PC2), it would be possible to use the EMG weighting coefficients to compute the temporal synergies. The failure of this analysis indicates that hand muscle synergies are fundamentally asynchronous.

Discussion

We demonstrated that within a single hand shape transition (i.e., moving from one stationary hand shape to another), different muscles become active at different times and for somewhat different durations. Thus, as previously demonstrated for arm-reaching movements (Flanders 1991, 2002; Flanders and others 1996), muscle activation waveforms are asynchronous and cannot be adequately described in terms of a single-command waveform acting as a common drive to groups of agonists and antagonists. On the other hand, also in consonance with our previous results for reaching movements (Flanders 1991; Flanders and others 1994), defining EMG levels as above (positive) or below (negative) the average level revealed instances of coactivation and reciprocal activation of muscle pairs. In the following sections, we will compare the present approach with other methods of synergy extraction, consider technical issues related to interpreting surface EMG signals, and, finally, speculate on the implications of the present results for the cortical control of hand movement.

Finding Muscle Synergies

Other investigators have sought to quantify synergies using various forms of PC analysis (e.g., Holdefer and Miller 2002; Brochier and others 2004; Ivanenko and others 2004), independent component analysis (e.g., Hart and Giszter 2004), and nonnegative matrix factorization (e.g., Tresch and others 1999; d'Avella and others 2003; d'Avella and Bizzi 2005; Ting and Macpherson 2005). We tend to prefer PC analysis because it produces a ranked set of orthogonal components and incorporates reciprocal patterns. Independent component analysis is well suited for studies where it is assumed that independent premotor drives are mixed in the EMG output and need to be untangled in the analysis. Nonnegative matrix factorization is a powerful, iterative curve-fitting method. It does not incorporate reciprocal patterns or assume the independence of premotor drives but instead tests for a small number of drives by using a search algorithm to extract specified numbers of muscle synergies and then measuring the goodness of fit to the EMG pattern.

Although the various computational strategies make different assumptions, the more important distinction between various approaches is whether a synergy is defined in terms of a single number for each muscle (synchronous synergy) or a temporal waveform for each muscle. This latter type of synergy was perhaps discovered by Nashner (1977), who showed a fixed distal to proximal bursting pattern in human leg muscles during a compensatory postural response. Much more recently, d'Avella and others have made major advances in this approach (d'Avella and others 2003; d'Avella and Bizzi 2005). An interesting aspect to their analysis is that 3 temporal synergies gave a good fit to data from frog leg movements if these synergies were scaled in amplitude and shifted in time (relative to one another) but not scaled in time. Hart and Giszter (2004) have also reported that frog EMG data contain bursts of fixed duration (about 275 ms), and although the temporal synergies of d'Avella and Bizzi (2005) sometimes featured different duration bursts for different muscles, it appears that the frog spinal cord may be prone to generate bursts, or sequences of bursts, of fixed duration.

In contrast, previous studies of arm EMG burst durations clearly showed time-base scaling depending on movement parameters such as speed (Gottlieb and others 1989; Buneo and others 1994). Furthermore, the EMG time base must scale in human gait because Ivanenko and others (2004) were able to identify 5 robust drive waveforms for synchronous synergies, only after EMG data from a wide range of locomotion speeds were timescaled into a unit-step cycle (meaning that the EMG bursts that result from the combination of these drives must scale in duration with the speed of locomotion). Interestingly, in a manner similar to the results of d'Avella and colleagues (d'Avella and others 2003; d'Avella and Bizzi 2005), some of the synchronous synergy waveforms of human locomotion were shifted later in time for slower locomotion speeds (Ivanenko and others 2004).

The temporal synergy approach employed in the present study was essentially similar to that of d'Avella and others (d'Avella and others 2003; d'Avella and Bizzi 2005). In fact, d'Avella and others (2003) also found one main temporal pattern that was present irrespective of the number of synergies specified in the extraction algorithm. In the present study, we did not test for time shifts and could not address the issue of timescaling. This is because even though we scaled letter-transition data into a single normalized time frame, these movements are naturally rhythmic, with a single main phase and nearly identical transition durations. However, in a previous study of reaching (Flanders 1991), we used an approach similar to that of Ivanenko and others (2004) and did find evidence for time shifts. We identified a single drive waveform that had to be scaled in amplitude and sometimes inverted in polarity to reconstruct EMG waveforms for arm movements in many different directions. However, it was only possible to derive this single robust drive waveform after the EMG waveforms associated with reaches in different directions were shifted in time to align them with one another. Thus, it appears that both time shifts and timescaling are essential features of human EMG patterns.

Interpreting EMG Signals

As mentioned in Materials and Methods, we assume that our bipolar surface electrodes record the units directly under the electrode with the largest amplitudes and more distant units with decrementally smaller amplitudes. Thus, it is important for us to position the electrodes directly over the muscle of interest. However, the motor units within that muscle do not receive a homogeneous drive (Herrmann and Flanders 1998; Weiss and Flanders 2004), and in fact during natural tasks, the discharge of pairs of motor units across different muscles may be as well correlated as pairs of motor units within the same muscle (Hockensmith and others 2005). Thus, our working hypothesis for the study of hand muscle synergies views the motor unit, and not the anatomically defined muscle, as the functional unit.

In our previous study (Weiss and Flanders 2004), we confirmed that with our very small, closely spaced electrodes, the chosen recording locations yield EMG data that are representative of the anatomical muscle of interest. This was done by discriminating single motor unit potentials from our surface recordings and then showing that the tuning curves for motor unit firing frequencies were similar to those for multiunit activity levels in the parent muscle. However, our previous study was on static hand shapes, and in the present study, EMG levels were much higher. Therefore, we need to emphasize that none of our present results or conclusions critically depend on the isolation of individual motor pools. In fact, as expected, DIT and DIF EMGs were very similar, and the 2 sets of electrodes certainly recorded from overlapping groups of motor units. In contrast, EMGs from the neighboring thumb muscles were sometimes similar and sometimes different. For example, in the nonrectified EMGs in the upper panels of Figure 3, APB and FPB show distinct bursting patterns. Likewise, the data from FD and FD2 were sometimes similar and sometimes distinct (rectified averaged EMGs in the lower panels of Fig. 3), indicating a good degree of isolation in the recordings.

Thus, we view the data recorded on each EMG channel as representing a spatially identified sample from a highly distributed network of motoneurons. We hypothesize that the network activity is directly shaped by peripheral sensory inputs and represents the ultimate output of activity in motor cortical areas. Thus, the temporal activation wave that we have illustrated here (in Fig. 9) may have implications for the organization of the hand area in motor cortex.

Speculating on Cortical Control

As mentioned in the Introduction, a major distinction between locomotion and hand movement is the degree of cortical involvement. A guiding concept in understanding motor cortical control of hand movement is that of somatotopy. Within the hand area of the somatotopic cortical map, there are multiple, partially overlapping patches representing each of the fingers, the thumb, and the wrist. This is true of both somatosensory and motor cortical areas (Hlustik and others 2001; Schieber 2001; Fitzgerald and others 2004). We have recently proposed that this is the pattern that would be expected if muscle synergies were mapped into a 2-dimensional (2D) space (Flanders 2005). This was mainly based on the study of Weiss and Flanders (2004), where we mapped 52 static hand shapes (17 joint angles) and the corresponding 52 static EMG patterns (8 muscles) into the orthogonal 2D space of the first 2 PCs (the postural and muscle synergies). We found a patchy, redundant representation of individual muscles and individual motor units within this 2D map.

Because these previous studies of somatotopic maps and muscle synergies were based mainly on simple electrical stimulation profiles or static postures, they now need to be extended to explain temporal patterns. Spinal networks may contribute to some of the temporal aspects of hand and arm motor patterns (Bizzi and others 2000), but there is also evidence for cortical involvement in generating patterned sequences of phasic motor commands (Fetz and others 1989; Graziano and others 2002; Park and others 2004). It may be that the patchy redundant somatotopy representing static muscle synergies is optimally organized to produce the appropriate spatial–temporal sequences of motor commands.

Notes

This work was supported by National Institutes of Health R01 NS027484. The authors thank Professor John F. Soechting for his many helpful suggestions. We also thank Philip Barbosa for assisting with our cadaver study and an anonymous reviewer for suggesting the sine wave analysis shown in Figure 9. *Conflict of Interest*: None declared.

Funding to pay the Open Access publication charges for this article was provided by the National Institute of Neurological Disorders and Stroke.

Address correspondence to Martha Flanders, Department of Neuroscience, 6-145 Jackson Hall, 312 Church Street Southeast, University of Minnesota, Minneapolis, MN 55455, USA. Email: fland001@umn.edu.

References

Basmajian JV, Blumenstein R. 1989. Electrode placement in electromyographic biofeedback. In: Basmajian JV, editor. Biofeedback: principles and practice for clinicians. 3rd ed. Baltimore, MD: Williams and Wilkins. p 369–382.

Basmajian JV, De Luca CJ. 1985. Muscles alive. 5th ed. Baltimore, MD: Williams and Wilkins.

Bizzi E, Giszter SF, Loeb E, Mussa-Ivaldi FA, Saltiel P. 1995. Modular organization of motor behavior in the frog's spinal cord. Trends Neurosci 18:442–446.

Bizzi E, Tresch MC, Saltiel P, d'Avella A. 2000. New perspectives on spinal motor systems. Nat Rev Neurosci 1:101–108.

Brochier T, Spinks RL, Umilta MA, Lemon R. 2004. Patterns of muscle activity underlying object-specific grasp by the Macaque monkey. J Neurophysiol 92:1770–1782.

Buchanan TS, Almdale DPJ, Lewis JL, Rymer WZ. 1986. Characteristics of synergic relations during isometric contractions in human elbow muscles. J Neurophysiol 56:1225–1241.

Buneo CA, Soechting JF, Flanders M. 1994. Patterns of muscle activation for reaching: the representation of distance and time. J Neurophysiol 71:1546–1558.

Burgar CG, Valero-Cuevas FJ, Hentz VR. 1997. Fine-wire electromyographic recordings during force generation: application to index finger kinesiologic studies. Am J P M R 76:494–501.

d'Avella A, Bizzi E. 2005. Shared and specific muscle synergies in natural motor behaviors. Proc Natl Acad Sci USA 102:3076–3081.

d'Avella A, Santiel P, Bizzi E. 2003. Contributions of muscle synergies in the construction of natural motor behavior. Nat Neurosci 6:300–308.

Fetz EE, Cheney PD, Mewes K, Palmer S. 1989. Control of forelimb muscle activity by populations of corticomotoneuronal and rubromotoneuronal cells. Prog Brain Res 80:437–449.

Fitzgerald PJ, Lane JW, Thakur PH, Hsiao SS. 2004. Receptive field properties of the macaque second somatosensory cortex: evidence for multiple functional representations. J Neurosci 24:11193–11204.

Flanders M. 1991. Temporal patterns of muscle activation for arm movements in three-dimensional space. J Neurosci 11:2680–2693.

Flanders M. 2002. Choosing a wavelet for single-trial EMG. J Neuorsci Methods 116:165–177.

Flanders M. 2005. Functional somatotopy in sensorimotor cortex. Neuroreport 16:313–316.

Flanders M, Pellegrini JJ, Geisler SD. 1996. Basic features of phasic activation for reaching in vertical planes. Exp Brain Res 110:67–79.

Flanders M, Pellegrini JJ, Soechting JF. 1994. Spatial/temporal characteristics of a motor pattern for reaching. J Neurophysiol 71:811–813.

Glaser EM, Ruchkin DS. 1976. Principles of neurobiological signal analysis. New York: Academic Press.

Gottlieb GL, Corcos DM, Agarwal GC. 1989. Strategies for the control of voluntary movements with one mechanical degree of freedom. Behav Brain Sci 12:189–250.

Graziano MS, Taylor CS, Moore T. 2002. Complex movements evoked by microstimulation of precentral cortex. Neuron 34:841–851.

Hart CB, Giszter SF. 2004. Modular premotor drives and unit bursts as primitives for frog motor behaviors. J Neurosci 24:5269–5282.

Herrmann U, Flanders M. 1998. Directional tuning of single motor units. J Neurosci 18:8402–8416.

Hlustik P, Solodkin A, Gullapalli RP, Noll DC, Small SL. 2001. Somatotopy in human primary motor and somatosensory hand representations revisited. Cereb Cortex 11:312–321.

Hockensmith GB, Soren YL, Fugelvand AJ. 2005. Common input across motor nuclei mediating precision grip in humans. J Neurosci 25:4560–4564.

Holdefer RN, Miller LE. 2002. Primary motor cortical neurons encode functional muscle synergies. Exp Brain Res 146:233–243.

Ivanenko YP, Poppele RE, Lacquaniti F. 2004. Five basic muscle activation patterns account for muscle activity during human locomotion. J Physiol 556:267–282.

Jerde TE, Soechting JF, Flanders M. 2003a. Biological constraints simplify the recognition of hand shapes. IEEE Trans Biomed Eng 50:265–269.

Jerde TE, Soechting JF, Flanders M. 2003b. Coarticulation in fluent fingerspelling. J Neurosci 23:2383–2393.

Macpherson J. 1991. How flexible are muscle synergies? In: Humphrey DR, Freund H-J, editors. Motor control: concepts and issues. New York: Wiley Press. p 33–47.

Nashner LM. 1977. Fixed patterns of rapid postural responses among leg muscles during stance. Exp Brain Res 30:13–24.

Oldfield RC. 1971. The assessment and analysis of handedness: the Edinburgh inventory. Neuropsychologia 9:97–113.

Park MC, Belhaj-Saif A, Cheney PD. 2004. Properties of primary motor cortex output to forelimb muscles in rhesus macaques. J Neurophysiol 92:2968–2984.

Saltiel P, Wyler-Duda K, D'Avella A, Tresch MC, Bizzi E. 2001. Muscle synergies encoded within the frog spinal cord: evidence from focal intraspinal NMDA iontophoresis in the frog. J Neurophysiol 85:605–619.

Santello M, Flanders M, Soechting JF. 1989. Postural hand synergies for tool use. J Neurosci 18:10105–10115.

Santello M, Flanders M, Soechting JF. 2002. Patterns of hand motion during grasping and the influence of sensory guidance. J Neurosci 22:1426–1435.

Schieber MH. 2001. Constraints on somatotopic organization in the primary motor cortex. J Neurophysiol 86:2125–2143.

Soechting JF, Flanders M. 1997. Flexibility and repeatability of finger movements during typing: analysis of multi-degree of freedom movements. J Comp Neurosci 41:29–46.

Soechting JF, Lacquaniti F. 1989. An assessment of the existence of muscle synergies during load perturbations and intentional movements of the human arm. Exp Brain Res 74:535–548.

Ting LH, Macpherson JM. 2005. A limited set of muscle synergies for force control during a postural task. J Neurophysiol 93:609–613.

Tresch MC, Saltiel P, Bizzi E. 1999. The construction of movement by the spinal cord. Nat Neurosci 2:162–167.

Weiss EJ, Flanders M. 2004. Muscular and postural synergies of the human hand. J Neurophysiol 92:523–535.